

Duplex: Dual Prototype Learning for Compositional Zero-Shot Learning

Zhong Peng^{1,2*}, Yishi Xu^{1*}, Gerong Wang^{1,2}, Wenchao Chen¹, Bo Chen^{1†}, Jing Zhang^{2†}

1.National Key Laboratory of Radar Signal Processing, Xidian University, Xi’an, China, 710071

2.Research Institute of Systems Engineering, Academy Military Science, Beijing, China, 100089

{mnspsz, xuyishi}@stu.xidian.edu.cn, bchen@mail.xidian.edu.cn

Abstract

Compositional Zero-Shot Learning (CZSL) enables models to recognize novel compositions of visual states and objects that not emerge during training. Existing methods struggle with generalization due to the complex entanglement of states and objects in visual representations, limiting their ability to handle unseen compositions. To address this challenge, we propose Duplex (Dual Prototype Learning), a novel approach that employs a well-designed dual-branch architecture to integrate both semantic and visual prototypes, thereby facilitating efficient composition learning. Duplex utilizes a graph neural network (GNN) to adaptively update visual prototypes, capturing intricate interactions between states and objects. It then leverages the strong visual-semantic alignment of pre-trained vision-language models (VLMs) and incorporates a multi-path architecture with prompt engineering to align image and text representations, ensuring robust generalization. Extensive experiments on three benchmark datasets—MIT-States, UT-Zappos, and C-GQA—demonstrate that Duplex outperforms the state of the art across all datasets in both closed-world and open-world settings.

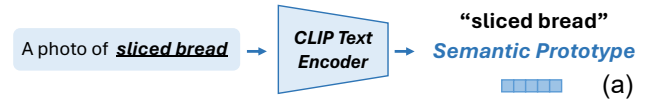
1. Introduction

Humans possess an extraordinary ability to understand and produce novel combinations from known concepts [1]. This compositional proficiency allows us to navigate various new scenarios seamlessly. For instance, for the first time we see a "black swan", we can readily recognize it by generalizing from our prior experiences with the animal "swan" and the color "black". Replicating this remarkable human trait in deep learning models is crucial to improve the adaptability and versatility of AI systems in complex and ever-changing real-world realities, where unseen concept combinations are evolving continuously and developing rapidly.

*Equal contribution

†Corresponding author

Unseen composition prompt



Seen composition image

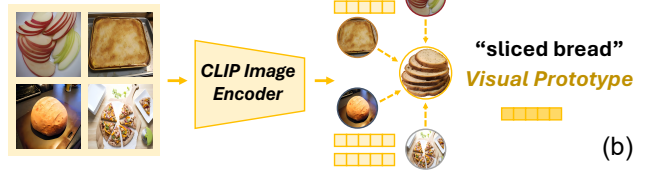


Figure 1. Motivation of our method. Augmenting semantic prototypes with visual prototypes enables a more comprehensive representation of compositions.

Compositional Zero-shot Learning (CZSL), aiming to equip models with the human-like generalization abilities, identifies *state-object* compositions that not emerge during training. This task is particularly challenging due to the inherent entanglement between the *state* and *object* within the context of an image. A successful CZSL model must not only learn the individual characteristics of *states* and *objects*, but also understand their complex interactions, and further extrapolate the combined knowledge to new, unseen compositions. This demand for generalization goes beyond the current boundaries of supervised learning paradigms, calling for innovative approaches that achieve efficient representation learning and precise compositional reasoning.

Early efforts [2–8] in CZSL have mainly centered around learning the combined *state-object* semantic representations to align with the visual features of images in a joint embedding space. This usually involves composing the individual semantic embeddings of *states* and *objects* using a certain transformation function, *e.g.*, a multi-layer perceptron (MLP) [2] or a graph convolutional network (GCN) [7, 8]. The underlying philosophy of this paradigm is that the combination rules learnt from seen compositions, expressed by the transformation function, can be transferred to unseen compositions effectively. Another line of research has fo-

cused on the disentanglement of visual concepts [9–13], building on the hypothesis that a good grasp over the primitive concepts of *states* and *objects* forms the basis for generalization to unseen compositions. This type of approach generally entails designing special disentangling modules to extract independent visual representations of *states* and *objects*, on which two separate classifiers are learned to recognize the *state* and *object*, respectively.

However, both of the above paradigms require learning to align image and text representations from scratch, which may compromise their generalization ability on unseen combinations, as much attention is paid to optimizing those compositions present during training. In addition, the task-specific architectures designed by these methods also limit their flexibility and scalability. Hence, recent studies have increasingly embraced pre-trained vision-language models (VLMs) such as CLIP [14] to tackle *CZSL*. Capitalizing on their inherent ability to generalize across diverse visual and linguistic concepts, existing VLM-based methods [15–19] have better flexibility while exhibiting impressive performance. However, these approaches concentrate heavily on refining the semantic embeddings of compositions, neglecting the enhancement of visual features and their potential role as a complementary source of information, which is crucial for achieving comprehensive understanding and recognition of novel compositions.

Recognizing the integral role of visual information in learning representations of unseen compositions, we propose a method that transcends the reliance solely on textual embeddings of states and objects. Instead, we advocate for a dual-aspect learning process where visual representations, derived directly from the disentangled image features, together with their textual counterparts form a comprehensive representation of the compositions. This approach emphasizes a holistic modeling strategy, enabling more accurate and robust object and state associations, thereby overcoming the limitations observed in traditional models and current VLM adaptations.

In summary, our main contributions are as follows:

- We present Duplex, a novel CLIP-based *CZSL* method that enables efficient generalization to unseen compositions by maintaining semantic and visual prototypical representations of the compositions.
- We propose an iterative learning strategy to refine the visual prototypes of compositions, which uses a graph neural network to adaptively aggregate the disentangled state and object visual features for updating prototypes.
- Extensive experimental results on three *CZSL* benchmark datasets demonstrate that Duplex achieves state-of-the-art (SOTA) performance in both closed-world and open-world settings.

2. Related Work

Compositional Zero-Shot Learning. *CZSL* is a major area of research. Existing methods for compositional zero-shot learning can be broadly divided into two categories. The first category includes approaches such as learning transformations for individual classifiers of states and objects [2], modeling each state as a linear transformation of objects [3], learning a hierarchical decomposition and composition of visual primitives [20], and modeling objects as invariant under attribute transformations [21]. Additionally, these methods include learning a joint compatibility function that accounts for the image, state, and object [4, 22]. To address the issue of generating unreasonable compositions from arbitrary combinations of states and objects, some works utilize external knowledge to filter out infeasible compositions [6, 23]. The second category newly proposed prompt-based methods utilize CLIP by replacing the classes in textual prompts with learnable state concept and object element embedding tokens [15]. DFSP [17] proposes a cross-modal decomposed fusion module that leverages soft prompts and a disentangling strategy to effectively capture more nuanced image features or use soft prefix vectors in the soft prompt [16]. the lasted Troika [18] proposing the Multi-Path explicitly modeling the state, object, and composition. In this work, we propose novelty method only uses object soft prompt to allow the model to learn composition relationships through graph connections futher boosting the unseen performance.

Vision-Language Models. VLMs [14, 24] are pre-trained to align semantic information across vision and language modalities, showing great promise in tasks such as visual question answering [25] and image caption [26]. Meanwhile, due to the prevalence of VLMs, prompt engineering enhance large pre-trained models like CLIP [27] and GPT-3 [28] by changing prompt guidance. Prompts can be static text or learnable word embeddings is introduced into multimodal settings to solve vision language related problems [29], including the *CZSL* problems [15, 17], aiming to help models quickly adapt to new tasks with little or none retraining. CLIP-based *CZSL* methods [15–17] extend prompt-tuning approach by fine-tuning both the inserted prefix and the primitive vocabulary tokens to better align with downstream semantic tasks.

3. The Proposed Method

Fig. 2 shows the framework of our Duplex. Next, we first define the problem formulation, and then present the details of each module of our method.

Problem formulation. To formally define the task of *CZSL*, we assume that there are two sets of primitive concepts, namely the state set and the object set, denoting them

as $\mathcal{S} = \{s_0, s_1, s_2, \dots, s_M\}$ and $\mathcal{O} = \{o_0, o_1, o_2, \dots, o_N\}$, respectively. Accordingly, the compositional label space \mathcal{C} is defined as their Cartesian product, *i.e.*, $\mathcal{C} = \mathcal{S} \times \mathcal{O}$, and hence the size of \mathcal{C} is derived as $M \times N$. Further dividing \mathcal{C} into two disjoint sets, where $\mathcal{C}_s \cup \mathcal{C}_u = \mathcal{C}$ and $\mathcal{C}_s \cap \mathcal{C}_u = \emptyset$, we obtain the set of seen classes \mathcal{C}_s during training, while the set of unseen classes \mathcal{C}_u are generally encountered during testing. Based on the scope of compositions covered at test time, CZSL can be categorized into 1) **the closed-world evaluation**, where the target set $\mathcal{C}_{tgt} = \mathcal{C}_s \cup \mathcal{C}'_u$ and \mathcal{C}'_u is a predefined subset of \mathcal{C}_u , *i.e.*, $\mathcal{C}'_u \subset \mathcal{C}_u$; 2) **the open-world evaluation**, where the target set contains all possible state-object compositions, *i.e.*, $\mathcal{C}_{tgt} = \mathcal{C}_s \cup \mathcal{C}_u = \mathcal{C}$.

For a given training set $\mathcal{T}_{tr} = \{(\mathbf{x}_i, c_i) \mid \mathbf{x} \in \mathcal{X}, c \in \mathcal{C}_s\}$, where \mathcal{X} denotes the input image space, the CZSL task aims to learn a model $f: \mathcal{X} \rightarrow \mathcal{C}_{tgt}$ to predict the label c of an input image $\mathbf{x} \in \mathcal{X}$ from the testing composition set \mathcal{T}_{te} .

3.1. Multi-path architecture

Learning Semantic Prototypes. Based on the success of previous works, learning effective semantic representations for compositions is essential to improve the performance of CZSL. The crux of this lies in constructing suitable prompts for compositional labels. Drawing on current winning practices, we employ a fully learnable soft prompt strategy, *i.e.*, we include a set of context vectors $\{\mathbf{v}_1^c, \dots, \mathbf{v}_K^c\}$ in front of word embeddings of each composition. Then, the resulting prompt $\mathbf{P}_{m,n}^c = \{\mathbf{v}_1^c, \dots, \mathbf{v}_K^c, \rho_m^s, \rho_n^o\}$ is fed into CLIP’s frozen text encoder to extract semantic prototypes, as shown in Fig. 2. Formally, this process is expressed as

$$\mathbf{t}_{m,n}^c = E_{txt}(\mathbf{P}_{m,n}^c) \quad (1)$$

With the semantic representations of compositions, it is still necessary to align them with the visual features of images to learn the optimal prompt that facilitates generalization. Thus, to obtain the image representation, we follow CLIP’s pre-processing routine to first rescale the image’s size to 224×224, and use ViT-L/14 as the image encoder to extract visual features. As the [CLS] token is exclusively used as a global representation of the input image for downstream tasks, here we take it directly as the target output.

$$\mathbf{z}_i^c = \mathbf{z}_i^{\text{cls}} = E_{img}(\mathbf{x}_i) \quad (2)$$

According to Eq. 1 and Eq. 2, we derive the visual feature \mathbf{z}_i^c of the input image \mathbf{x}_i and the semantic representations of all compositions, which allows us to compute the probability that \mathbf{x}_i belongs to its corresponding compositional label $c_i = (s_m, o_n)$. The formulation could be written as

$$p(c_{m,n} \mid \mathbf{x}) = \frac{\exp(\mathbf{z}^c \cdot \mathbf{t}_{m,n}^c / \tau)}{\sum_{n=1}^N \sum_{m=1}^M \exp(\mathbf{z}^c \cdot \mathbf{t}_{m,n}^c / \tau)} \quad (3)$$

The cross-entropy loss encourages the model to recognize the corresponding semantic role, described as:

$$\mathcal{L}_c = -\frac{1}{|\mathcal{X}|} \sum_{\mathbf{x} \in \mathcal{X}} \log p(c_{m,n} \mid \mathbf{x}) \quad (4)$$

Disentangling Visual Representations. As we discussed, maintaining only semantic prototype representations for compositional labels results in a limited generalization ability of the model. On the one hand, the model may overfit those seen compositional labels, as only their prompts are explicitly optimized. On the other hand, in terms of textual descriptions, the semantic differences among compositional labels may be very subtle, rendering them indistinguishable in the representation space. Thus, a good alternative is to seek visual prototype representations of compositions from the image information flow.

However, states and objects are intrinsically entangled in the context of images. In order to learn rational visual prototypes for both seen and unseen compositions, we have to disentangle the state information and the object content. This enables us to acquire visual prototype representations of any compositions by designing fusion mechanisms to aggregate the separate features of states and objects flexibly. To this end, we design two disentanglers, D^s and D^o , to separate the visual features of states and objects, respectively, from the global representation ([CLS] token) of the image.

$$\mathbf{z}_i^s = D^s(\mathbf{z}_i^{\text{cls}}); \mathbf{z}_i^o = D^o(\mathbf{z}_i^{\text{cls}}) \quad (5)$$

where both $D^s(\cdot)$ and $D^o(\cdot)$ are implemented using two distinct double-layer MLPs.

It is worth noting that the direct incorporation of D^s and D^o does not lead to the effect of disentanglement. Rather, it requires the aid of a supervised signal to facilitate specialization. Therefore, we construct prompts for states and objects in a similar way to compositions. Formally, we have

$$\begin{aligned} \mathbf{t}_m^s &= E_{txt}(\mathbf{P}_m^s) = E_{txt}(\{\mathbf{v}_1^s, \dots, \mathbf{v}_K^s, \rho_m^s\}) \\ \mathbf{t}_n^o &= E_{txt}(\mathbf{P}_n^o) = E_{txt}(\{\mathbf{v}_1^o, \dots, \mathbf{v}_K^o, \rho_n^o\}) \end{aligned} \quad (6)$$

With the semantic representations of states and objects, we similarly align them with corresponding visual features by jointly maximizing the probability of the true state or object to which the image belongs, which could be formulated as

$$\begin{aligned} p(s_m \mid \mathbf{x}) &= \frac{\exp(\mathbf{z}^s \cdot \mathbf{t}_m^s / \tau)}{\sum_{m=1}^M \exp(\mathbf{z}^s \cdot \mathbf{t}_m^s / \tau)} \\ p(o_n \mid \mathbf{x}) &= \frac{\exp(\mathbf{z}^o \cdot \mathbf{t}_n^o / \tau)}{\sum_{n=1}^N \exp(\mathbf{z}^o \cdot \mathbf{t}_n^o / \tau)} \end{aligned} \quad (7)$$

$$\begin{aligned} \mathcal{L}_s &= -\frac{1}{|\mathcal{X}|} \sum_{\mathbf{x} \in \mathcal{X}} \log p(s_m \mid \mathbf{x}) \\ \mathcal{L}_o &= -\frac{1}{|\mathcal{X}|} \sum_{\mathbf{x} \in \mathcal{X}} \log p(o_n \mid \mathbf{x}) \end{aligned} \quad (8)$$

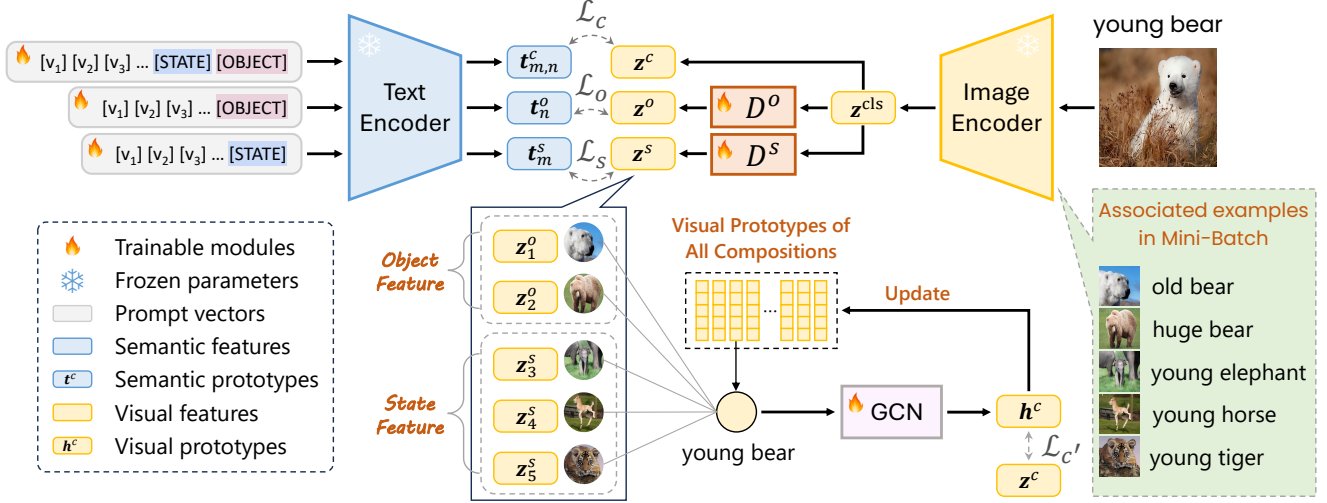


Figure 2. Overview of our proposed *Duplex*. The *Duplex* framework consists of two parts: the semantic prototype module and the visual prototype module. The semantic prototype part is responsible for extracting linguistic features, while the visual prototype part is responsible for extracting the same state and object image features through seen compose categories and generalizing them to unseen compose categories.

By now we have found that our architecture coincides with the multi-path paradigm proposed by [18]. However, the two additional branches we have here are designed to promote efficient learning of visual prototypes later on.

3.2. Dual prototype learning

Graph-based Visual Prototypes Learning. we maintain a global codebook to store the visual prototype vectors of all possible compositions, denoted as $\mathbf{H} = \{h_1^c, \dots, h_{M \times N}^c\}$. These prototype vectors are randomly initialized but can be progressively refined throughout the training process. Our approach innovatively incorporates the graph convolutional network (GCN) [30] to update the visual prototypes of compositions and learn adaptive fusion rules, as shown in Fig. 2. Specifically, within a mini-batch, for each composition in the codebook, we identify and select all image samples that share either the state, the object, or both with the given composition, given that the compositional labels of the training samples are known. From these selected images, we extract their state visual features $\mathbf{Z}^s = \{z_1^s, \dots, z_m^s\}$ and object visual features $\mathbf{Z}^o = \{z_1^o, \dots, z_n^o\}$, respective.

Based on this, we build a graph centered on the prototype representation of a given composition, connected to which are many visual features closely related to it. This graph is then fed into a GCN for knowledge propagation, allowing the model to leverage the structural information and interactions among the features. Then the refined and contextually enriched prototype vector is derived as

$$\hat{h}_j^c = \text{GCN}(h_j^c; \mathbf{Z}^s, \mathbf{Z}^o) \quad (9)$$

The prototype vectors produced by the GCN not only

serve to update their corresponding counterparts in the codebook, but also requires some regularization to align with the global representation of the image, thereby ensuring it is iteratively optimized in a constructive direction.

$$p(c'_{m,n} | \mathbf{x}) = \frac{\exp(\mathbf{z}^c \cdot \mathbf{h}^c / \tau)}{\sum_{n=1}^N \sum_{m=1}^M \exp(\mathbf{z}^c \cdot \mathbf{h}^c / \tau)} \quad (10)$$

$$\mathcal{L}_{c'} = -\frac{1}{|\mathcal{X}|} \sum_{\mathbf{x} \in \mathcal{X}} \log p(c'_{m,n} | \mathbf{x}) \quad (11)$$

3.3. Overall objective and inference

At the training phase, we formulate our final loss as cross-entropy loss encourages the model to explicitly recognize the corresponding semantic role, described as:

$$\mathcal{L} = \mathcal{L}_s + \mathcal{L}_o + \mathcal{L}_c + \mathcal{L}_{c'} \quad (12)$$

At the inference phase, we feed the same test input, deriving four class probabilities $p(c')$, $p(c)$, $p(s)$, and $p(o)$, where $c = (s, o)$, $c' = c_{text} + c_{visual}$. Unlike most methods modeling single $p(c)$ for prediction, we compute our prediction score by synthesizing composed composition, and integrated composition probability $\tilde{p}(c_{m,n} | \mathbf{x})$ is defined as

$$\tilde{p}(c_{m,n} | \mathbf{x}) = p(c'_{m,n} | \mathbf{x}) + p(c_{m,n} | \mathbf{x}) + p(s_m | \mathbf{x}) \cdot p(o_n | \mathbf{x}) \quad (13)$$

The joint distribution of composition probabilities, assuming attribute and object predictions are independent, is

treated as a bias correction for the direct prediction of compositions. The most likely composition can then be predicted as follows:

$$\tilde{c} = \arg \max_{c_{m,n} \in \mathcal{C}_{tgt}} \tilde{p}(c_{m,n} | \mathbf{x}) \quad (14)$$

where \tilde{c} denotes the predicted composed label.

4. Experimental Evaluation

4.1. Experimental setup

Dataset. We conduct our experiments on three real-world CZSL benchmarks, including MIT-States [32], UT-Zappos [33], and C-GQA [7], and follow the split suggested by previous works. Specifically, the MIT-States dataset comprises 53753 natural images, featuring 115 states and 245 objects. Within the closed-world settings, the search space encompasses 1262 seen compositions, as well as 300 unseen compositions for validation and 400 unseen compositions for testing. The UT-Zappos dataset consists of 50025 images of shoes, characterized by 16 states and 12 objects. For closed-world experiments, it is limited to 83 seen compositions and 15/18 unseen compositions (for validation and testing, respectively). Regarding the CGQA dataset, which is the most extensive pairs dataset for CZSL, it contains 453 states and 870 objects, with a total of 39298 images, which includes over 9500 compositions. In open-world settings, these datasets contain 28175, 192 and 278362 compositions.

Benchmark Metrics Following previous works [4, 7, 10, 15], we follow the standard of adding a scalar bias to the seen and unseen classes at test time. Varying the candidate bias from $-\infty$ to $+\infty$ to get a curve can be drawn with the accuracy of seen on the x-axis and unseen on the y-axis pairs. Following prior work, we compute the area under the curve (AUC) and select the point with the best harmonic mean (HM) between the seen and unseen accuracy. We also report the best seen accuracy (S) by setting the bias to $-\infty$, and the best unseen accuracy (U) by setting the bias to $+\infty$. We select the best-performing model on validation data.

Baseline and Training Details In our experiments, we primarily compare the *Duplex* method with various CLIP-based baselines. Specifically, we evaluate *Duplex* against pre-trained CLIP [14], CoOp [31], CSP [15], GIPCOL [16], and all versions of DFSP [17]. All comparison methods use the CLIP model ViT-L/14, which is the largest available model in the experiments. We train all our models on a single NVIDIA A800 GPU, minimizing the cross-entropy loss with the Adam optimizer, and conduct training over the seen split of the dataset for 20 epochs.

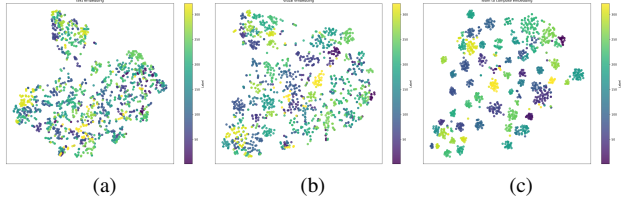


Figure 3. Embedding visualization. Embedding visualization was conducted by selecting the first 300 classes from the MIT-States dataset for clustering, with colors representing different categories. Embedding visualization was performed separately for (a) semantic prototype embedding, (b) visual prototype embedding, and (c) the combined joint semantic and visual prototypes embedding.

4.2. Experimental results

In this section, we compare our proposed *Duplex* to CLIP-based baselines in the closed-world and open-world settings of compositional zero-shot learning. We report the closed-world and the open-world results. As in Table 9, under the closed-world setting, our method achieved new state-of-the-art (SOTA) performance on the MIT-States, UT-Zappos, and C-GQA datasets. Specifically, our method attained the highest AUC scores of 23.7% on MIT-States, 45.5% on UT-Zappos, and 13.2% on C-GQA. Compared to existing methods, we improved the harmonic mean by 1.6% on MIT-States. Additionally, our method demonstrated superior visible and invisible accuracy across these datasets. The substantial improvement on UT-Zappos highlights our model’s capability to accurately extract visual prototypes, which may be particularly effective for data in specialized domains. Overall, our model exhibited strong performance across all datasets.

Similarly, as shown in Table 10, our method also achieved SOTA results for these three datasets under the open-world setting. On UT-Zappos, our method outperformed Troika by 2.4% in the AUC metric. The unseen accuracy in the open-world setting showed significant improvement, increasing by 1.5% on MIT-States and 1.3% on C-GQA. These results indicate that our method provides consistent and comprehensive performance through the joint utilization of semantic and visual prototypes.

4.3. Ablation study

Ablation on semantic and visual prototype module.

The purpose of this ablation study is to evaluate the effectiveness of the visual prototype learning module and the semantic prototype learning module, which includes multi-path prompt learning, the visual prototype module (VP), and the semantic prototype module (SP). The results of the ablation study are presented in Table 3, targeting the closed-world datasets UT-Zappos and MIT-State. The results in row (0) indicate that multi-path prompts demon-

Method	MIT-States				UT-Zappos				CGQA			
	S	U	HM	AUC	S	U	HM	AUC	S	U	HM	AUC
CLIP [14]	30.2	46.0	26.1	11.0	15.8	49.1	15.6	5.0	7.5	25.0	8.6	1.4
CoOp [31]	34.4	47.6	29.8	13.5	52.1	49.3	34.6	18.8	20.5	26.8	17.1	4.4
CSP [15]	46.6	49.9	36.3	19.4	64.2	66.2	46.6	33.0	28.8	26.8	20.5	6.2
GIPCOL [16]	48.5	49.6	36.6	19.9	65.0	68.5	48.8	36.2	31.92	28.4	22.5	7.14
DFSP(i2t) [17]	47.4	52.4	37.2	20.7	64.2	66.4	45.1	32.1	35.6	29.3	24.3	8.7
DFSP(BiF) [17]	47.1	52.8	37.7	20.8	63.3	69.2	47.1	33.5	36.5	32.0	26.2	9.9
DFSP(t2i) [17]	46.9	52.0	37.3	20.6	66.7	71.7	47.2	36.0	38.2	32.0	27.1	10.5
Troika [18]	49.0	53.0	39.3	22.1	66.8	73.8	54.6	41.7	41.0	35.7	29.4	12.4
Duplex(ours)	49.7	55.6	40.9	23.7	70.2	74.7	57.3	45.5	41.1	36.2	30.1	13.2

Table 1. Main Results in a Closed-World Setting on Three Benchmarks. All methods use a CLIP ViT-L/14 backbone.

Method	MIT-States				UT-Zappos				CGQA			
	S	U	HM	AUC	S	U	HM	AUC	S	U	HM	AUC
CLIP [14]	30.1	14.3	12.8	3.0	15.7	20.6	11.2	2.2	7.5	4.6	4.0	0.27
CoOp [31]	34.6	9.3	12.3	2.8	52.1	31.5	28.9	13.2	21.0	4.6	5.5	0.70
CSP [15]	46.3	15.7	17.4	5.7	64.1	44.1	38.9	22.7	28.7	5.2	6.9	1.20
GIPCOL [16]	48.5	16.0	17.9	6.3	65.0	45.0	40.1	23.5	31.6	5.5	7.3	1.30
DFSP(i2t)[17]	47.2	18.2	19.1	6.7	64.3	53.8	41.2	26.4	35.6	6.5	9.0	1.95
DFSP(BiF) [17]	47.1	18.1	19.2	6.7	63.5	57.2	42.7	27.6	36.4	7.6	10.6	2.39
DFSP(t2i)[17]	47.5	18.5	19.3	6.8	66.8	60.0	44.0	30.3	38.3	7.2	10.4	2.40
Troika [18]	48.8	18.7	20.1	7.2	66.4	61.2	47.8	33.0	40.8	7.9	10.9	2.70
Duplex(ours)	49.5	20.3	21.8	8.3	70.2	62.4	49.6	35.4	41.6	9.2	12.5	3.9

Table 2. Main Results in a Open-World Setting on Three Benchmarks. All methods use a CLIP ViT-L/14 backbone.

Module	MIT-States				UT-Zappos						
	c-s-o	SP	VP	S	U	HM	AUC	S	U	HM	AUC
(0)	✓	✗	✗	48.6	49.8	36.8	20.1	64.4	70.7	51.9	37.8
(1)	✓	✓	✗	49.0	52.4	37.9	21.7	66.9	74.5	54.7	42.1
(2)	✓	✗	✓	49.4	52.1	38.5	21.9	68.1	72.9	56.3	43.7
(3)	✓	✓	✓	49.7	55.6	40.9	23.7	70.2	74.7	57.3	45.5

Table 3. Ablate the components in *Duplex* on the close-world dataset UT-Zappos and MIT-State. c-s-o, SP, and VP denote composition, state, and object prompt, VP denotes the visual prototype Module, SP denotes the semantic prototype Module.

Inference formulation	S	U	HM	AUC
(0) $p(s) \cdot p(o)$	45.7	34.2	26.1	11.3
(1) $p(c)$	50.5	47.8	36.8	20.1
+ $p(s) \cdot p(o)$	49.4	51.3	37.6	21.2
(2) $p(c')$	42.6	45.6	32.6	15.8
+ $p(s) \cdot p(o)$	45.8	47.1	33.8	17.5
(3) $p(c') + p(c)$	51.2	54.0	39.3	22.9
+ $p(s) \cdot p(o)$	49.7	55.6	40.9	23.7

Table 4. Results on closed-world datasets MIT-State using different inference formulations. Rows (0)-(2) respectively represent the cases when use product of state and object probabilities $p(s) \cdot p(o)$, semantic prototype $p(c)$ and compose composition $p(c')$. Row (3) is our inference formulation, can achieve best performance.

strate greater effectiveness compared to other methods. In this study, we utilize the multi-path prompt method proposed in [18] as the baseline model. Rows (1) and (2) in-

dicating that using the semantic prototype learning module or the visual prototype learning module can improve the overall performance of the model. Visualization Fig.3 shows the stronger capability of the *Duplex* combined features, from the perspective of feature complementarity, as shown in Fig. 3a and 3b, visual features show a relative advantage in classification compared to standalone text semantic features. Due to the complementary nature of the two modalities, as illustrated in Fig. 3c, combining them through LTC yields notable classification improvements. Row (3) indicates that the combined use of semantic and visual modules can further optimize combined performance, thereby improving unseen accuracy and overall AUC.

Ablation on Inference formulation. We investigate the impact of inference formulation $p(c') + p(c) + p(s) \cdot p(o)$, as shown in Table 4. Specifically, $p(c')$ and $p(c)$ represent predictions made using only semantic or visual prototype probabilities, while $p(s) \cdot p(o)$ denotes the product of state and object probabilities. Notably, good performance can be achieved using only $p(c')$ or $p(c)$, and it is clear when examining the MIT-State dataset that using only $p(s) \cdot p(o)$ is not a reliable predictor. However, integrating $p(s) \cdot p(o)$ into the composite model $p(c') + p(c)$ significantly improves the accuracy of unseen inference. These findings emphasize the importance of learning state and target combina-

tions through semantic or visual prototypes in enhancing generalization capabilities in the context of the Composite Zero-shot Learning (CZSL) problem.

Loss formulation	S	U	HM	AUC
(0) $\mathcal{L}_s + \mathcal{L}_o$	30.4	54.4	30.8	13.1
(1) \mathcal{L}_c	67.2	68.0	56.4	42.0
+ $(\mathcal{L}_s + \mathcal{L}_o)$	68.5	73.2	57.1	44.9
(2) \mathcal{L}_c	66.9	68.9	52.1	39.6
+ $(\mathcal{L}_s + \mathcal{L}_o)$	68.4	71.2	54.5	40.3
(3) $\mathcal{L}_c + \mathcal{L}_c$	70.7	74.2	57.1	45.1
+ $(\mathcal{L}_s + \mathcal{L}_o)$	70.2	74.7	57.3	45.5

Table 5. Results on closed-world datasets UT-Zappos. Rows(0) means use state and object logits for training, Rows(1)-Rows(2) means use visual prototype and semantic prototype for training. Rows(3) represent our best loss function.

update strategy	MIT-States				CGQA			
	S	U	HM	AUC	S	U	HM	AUC
(0) \mathcal{N}_{init}	48.9	49.9	37.4	20.4	41.3	33.6	26.6	11.8
(1) \mathcal{N}_{batch}	46.8	51.1	36.9	19.9	40.1	34.0	28.5	11.6
(2) $\lambda \cdot \mathcal{N}_{init} + (1 - \lambda) \cdot \mathcal{N}_{batch}$	49.7	55.6	40.9	23.7	41.1	36.2	30.1	13.2

Table 6. Results on closed-world datasets MIT-States and CGQA using different strategy update state and object node feature for composition. Rows (0)-(1) respectively represent the cases when $\lambda = 1$ and $\lambda = 0$. Row (2) is our inference formulation, which applies a λ optimized on the validation set.

Ablation on Loss formulation. The proposed loss formulation demonstrates superior results on the UT-Zappos dataset under a closed-world setting, as shown in Tab.5. Our approach outperforms other configurations by enhancing visual and semantic prototype features and incorporating state and object as regularization terms during model training. This enables *Duplex* to capture the influence of state-object pairs in each image, thereby enhancing model performance.

Ablation on visual prototype update. We examined the impact of the update strategy $(\lambda \cdot \mathcal{N}_{init} + (1 - \lambda) \cdot \mathcal{N}_{batch})$, as shown in Table 6. We specifically report the results for the extreme values of λ , namely $\lambda = 0.0$ and $\lambda = 1.0$. For $\lambda = 1.0$, CLIP encodes the images to separately derive the visual average features of states and objects before updating *Duplex*. Conversely, $\lambda = 0.0$ employs randomly initialized state and object nodes, updating *Duplex* based on the states and objects present in each training batch. Our findings indicate that the optimal fixed value varies among different datasets. The results on MIT-State and CGQA reveal that using either \mathcal{N}_{init} or \mathcal{N}_{batch} alone to obtain visual prototypes does not outperform the combined approach, except for a slightly high metric seen on CGQA with \mathcal{N}_{init} . Therefore, choosing λ based on validation set performance yields the best results, with $\lambda = 0.9$ being the optimal value for the MIT-State dataset.

4.4. Qualitative visualization

Inspired by previous work[12, 13, 34], we conduct a qualitative analysis of image and text retrieval to demonstrate how our *Duplex* model correlates images and text.

Image to Composition. In Fig.4, we present qualitative results from the test sets of the MIT-States, UT-Zappo, and CGQA datasets, which include both seen and unseen compositions. Given an image, such as an ‘‘ancient house’’ we extract its visual prototype features and retrieve the top three similar text composition embeddings. Although identifying the true label within the top-ranked text compositions is challenging, all top three results are semantically related to the image.

For instance, in the image of ‘‘folded pizza’’ (row 1, column 4), while ‘‘folded pizza’’ does not appear among the top three matches, the retrieved results ‘‘crushed tomato’’ and ‘‘diced cheese’’ are reasonable and visually present in the image. The same observation applies to the image of a ‘‘gray animal’’ (row 3, column 4). Despite differing from the provided labels, these complete prediction errors provide an alternative effectiveness and surpass traditional metrics. The composition predictions validate that our model effectively identifies visual and related semantic features.

Semantic and Visual retrieval. First, we consider semantic-to-visual retrieval. Given a semantic prototype feature obtained through *Duplex*, such as ‘‘Suede Slippers’’ (row 2), we embed it and retrieve the four most similar images based on feature distance. The left side of Fig.5 (Image retrieval using semantic prototype) illustrates four different objects sharing the same textual composition.

Next, we examine visual prototype feature-to-image retrieval, as shown on the right side of Fig.5 (Image retrieval using visual prototype). For instance, we extract the ‘‘Suede Slippers’’ visual prototype feature and retrieve the top four similar images, where all results are based on the visual prototype.

Our observations indicate that images retrieved using visual prototype features from *Duplex* are generally accurate. However, semantic prototype retrieval may yield exceptions; for example, when retrieving ‘‘Suede Slippers,’’ the second closest image might be ‘‘Canvas Loafers.’’ While ‘‘Suede Slippers’’ and ‘‘Canvas Loafers’’ are not the same composition in semantic retrieval, visual-prototype searches yield more similar and correct images. The same applies to the composition of a ‘‘Brown Horse’’ (row 3). These retrieval experiments demonstrate that our visual prototype effectively captures the intended compositions and compensates for the biases inherent in the semantic prototype.



Figure 4. Qualitative results. We randomly selected cases from MIT-States (the top row), UT-Zappos (the mid row) and CGQA (the bottom row). Each image has the ground-truth label (black text) and three predict results (colored text), in which the green text is the correct prediction.

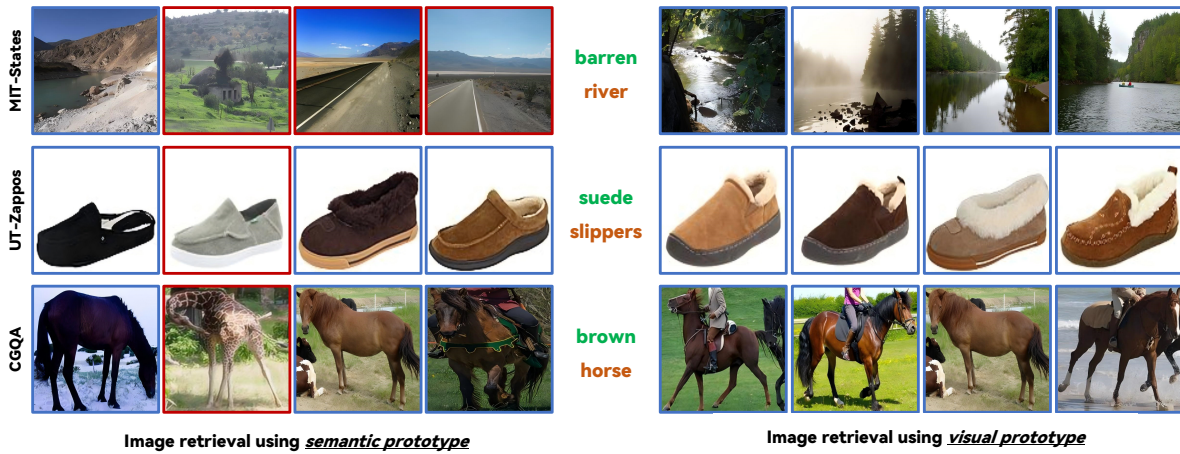


Figure 5. Semantic and Visual Prototype Retrieval. We conduct retrieval using semantic and visual prototypes extracted via Duplex on three datasets. In the first row, the incorrect result (highlighted in red) is 'barren road'. In the second row, the incorrect result is 'canvas loafers'. In the third row, the incorrect result is 'brown giraffe'.

4.5. Why Duplex can work well?

Extensive experimental studies demonstrate the effectiveness of Duplex, and we provide an in-depth analysis of the underlying reasons. First, as shown in previous research, text and image encoders have been pre-trained on large-scale image-text pair datasets. These encoders can be effectively fine-tuned using prompt-based learning, significantly improving model performance. Second, from the perspective of feature complementarity, visual features, as illustrated in Fig. 5, exhibit a relative advantage in classification compared to standalone text semantic features. Duplex learning can classify state and object features through semantic and visual prototypes. This approach establishes relationships between unseen image information and state-objects, enabling performance that surpasses compositions seen during training.

Notably, we observe substantial performance improvements in experiments conducted on smaller or domain-

specific datasets. Duplex enhances the classification of specific domain states and objects, likely due to reduced ambiguity within the domain regarding these states and objects, which enables the model to learn more robust features. However, when working with more general datasets, we found that a significant number of mislabeling issues (i.e., image-label mismatches) somewhat limited the model's performance gains on larger datasets. In summary, Duplex learning, by composing features through visual and semantic prototypes, enhances the model's sensitivity to unseen compositions.

5. Conclusion

In this paper, we have proposed a novel approach, named *Duplex* (Dual Prototype Learning), for compositional zero-shot learning based on CLIP. Specifically, by designing a dual-branch structure, we integrate both semantic and visual prototypes into the *Duplex*, enhancing its

generalization ability of vision-language models for unseen combinations significantly. Extensive experiments on three widely-used CZSL benchmark datasets—UT-Zappos, MIT-States, and C-GQA—demonstrate that the Duplex method achieves substantial performance improvements in both closed-world and open-world settings, outperforming current state-of-the-art methods.

References

- [1] Brenden M Lake and Marco Baroni. Human-like systematic generalization through a meta-learning neural network. *Nature*, 623(7985):115–121, 2023. 1
- [2] Ishan Misra, Abhinav Gupta, and Martial Hebert. From red wine to red tomato: Composition with context. In *2017 IEEE Conference on Computer Vision and Pattern Recognition (CVPR)*, pages 1160–1169, 2017. doi: 10.1109/CVPR.2017.129. 1, 2
- [3] Tushar Nagarajan and Kristen Grauman. Attributes as operators: Factorizing unseen attribute-object compositions. In *Computer Vision – ECCV 2018: 15th European Conference, Munich, Germany, September 8–14, 2018, Proceedings, Part I*, page 172–190, Berlin, Heidelberg, 2018. Springer-Verlag. ISBN 978-3-030-01245-8. doi: 10.1007/978-3-030-01246-5_11. URL https://doi.org/10.1007/978-3-030-01246-5_11. 2, 4
- [4] Senthil Purushwalkam, Maximilian Nickel, Abhinav Gupta, and Marc’Aurelio Ranzato. Task-driven modular networks for zero-shot compositional learning. In *Proceedings of the IEEE/CVF International Conference on Computer Vision (ICCV)*, October 2019. 2, 5
- [5] Yong-Lu Li, Yue Xu, Xiaohan Mao, and Cewu Lu. Symmetry and group in attribute-object compositions. In *Proceedings of the IEEE/CVF conference on computer vision and pattern recognition*, pages 11316–11325, 2020.
- [6] M Mancini, MF Naeem, Y Xian, and Zeynep Akata. Open world compositional zero-shot learning. In *34th IEEE Conference on Computer Vision and Pattern Recognition*. IEEE, 2021. 2, 4
- [7] MF Naeem, Y Xian, F Tombari, and Zeynep Akata. Learning graph embeddings for compositional zero-shot learning. In *34th IEEE Conference on Computer Vision and Pattern Recognition*. IEEE, 2021. 1, 5, 4
- [8] Massimiliano Mancini, Muhammad Ferjad Naeem, Yongqin Xian, and Zeynep Akata. Learning graph embeddings for open world compositional zero-shot learning. *IEEE Transactions on pattern analysis and machine intelligence*, 46(3): 1545–1560, 2022. 1, 4
- [9] Frank Ruis, Gertjan Burghouts, and Doina Bucur. Independent prototype propagation for zero-shot compositionality. *Advances in Neural Information Processing Systems*, 34: 10641–10653, 2021. 2
- [10] Tian Zhang, Kongming Liang, Ruoyi Du, Xian Sun, Zhanyu Ma, and Jun Guo. Learning invariant visual representations for compositional zero-shot learning. In *Computer Vision – ECCV 2022: 17th European Conference, Tel Aviv, Israel, October 23–27, 2022, Proceedings, Part XXIV*, page 339–355, Berlin, Heidelberg, 2022. Springer-Verlag. ISBN 978-3-031-20052-6. doi: 10.1007/978-3-031-20053-3_20. URL https://doi.org/10.1007/978-3-031-20053-3_20. 5
- [11] Xiangyu Li, Xu Yang, Kun Wei, Cheng Deng, and Muli Yang. Siamese contrastive embedding network for compositional zero-shot learning. In *Proceedings of the IEEE/CVF Conference on Computer Vision and Pattern Recognition (CVPR)*, pages 9326–9335, June 2022. 4
- [12] Nirat Saini, Khoi Pham, and Abhinav Shrivastava. Disentangling visual embeddings for attributes and objects. In *Proceedings of the IEEE/CVF Conference on Computer Vision and Pattern Recognition (CVPR)*, pages 13658–13667, June 2022. 7
- [13] Shaozhe Hao, Kai Han, and Kwan-Yee K. Wong. Learning attention as disentangler for compositional zero-shot learning. In *Proceedings of the IEEE/CVF Conference on Computer Vision and Pattern Recognition (CVPR)*, pages 15315–15324, June 2023. 2, 7, 4
- [14] Alec Radford, Jong Wook Kim, Chris Hallacy, Aditya Ramesh, Gabriel Goh, Sandhini Agarwal, Girish Sastry, Amanda Askell, Pamela Mishkin, Jack Clark, Gretchen Krueger, and Ilya Sutskever. Learning transferable visual models from natural language supervision. In Marina Meila and Tong Zhang, editors, *Proceedings of the 38th International Conference on Machine Learning*, volume 139 of *Proceedings of Machine Learning Research*, pages 8748–8763. PMLR, 18–24 Jul 2021. URL <https://proceedings.mlr.press/v139/radford21a.html>. 2, 5, 6, 4
- [15] Nihal V. Nayak, Peilin Yu, and Stephen H. Bach. Learning to compose soft prompts for compositional zero-shot learning. In *International Conference on Learning Representations*, 2023. 2, 5, 6, 4
- [16] Guangyue Xu, Joyce Chai, and Parisa Kordjamshidi. Gipcol: Graph-injected soft prompting for compositional zero-shot learning. In *2024 IEEE/CVF Winter Conference on Applications of Computer Vision (WACV)*, pages 5762–5771, 2024. doi: 10.1109/WACV57701.2024.00567. 2, 5, 6, 4
- [17] Xiaocheng Lu, Song Guo, Ziming Liu, and Jingcai Guo. Decomposed soft prompt guided fusion enhancing for compositional zero-shot learning. In *Proceedings of the IEEE/CVF Conference on Computer Vision and Pattern Recognition (CVPR)*, pages 23560–23569, June 2023. 2, 5, 6, 4
- [18] Siteng Huang, Biao Gong, Yutong Feng, Min Zhang, Yiliang Lv, and Donglin Wang. Troika: Multi-path cross-modal traction for compositional zero-shot learning. In *Proceedings of the IEEE/CVF Conference on Computer Vision and Pattern Recognition*, 2024. 2, 4, 6
- [19] Guangyue Xu, Parisa Kordjamshidi, and Joyce Chai. Prompting large pre-trained vision-language models for compositional concept learning. *arXiv preprint arXiv:2211.05077*, 2022. 2
- [20] Muli Yang, Cheng Deng, Junchi Yan, Xianglong Liu, and Dacheng Tao. Learning unseen concepts via hierarchical decomposition and composition. In *Proceedings of the IEEE/CVF Conference on Computer Vision and Pattern Recognition*, pages 10248–10256, 2020. 2

- [21] Yong-Lu Li, Yue Xu, Xiaohan Mao, and Cewu Lu. Symmetry and group in attribute-object compositions. In *Proceedings of the IEEE/CVF Conference on Computer Vision and Pattern Recognition (CVPR)*, June 2020. 2
- [22] Yuval Atzmon, Felix Kreuk, Uri Shalit, and Gal Chechik. A causal view of compositional zero-shot recognition. In H. Larochelle, M. Ranzato, R. Hadsell, M.F. Balcan, and H. Lin, editors, *Advances in Neural Information Processing Systems*, volume 33, pages 1462–1473. Curran Associates, Inc., 2020. URL https://proceedings.neurips.cc/paper_files/paper/2020/file/1010cedf85f6a7e24b087e63235dc12e-Paper.pdf. 2
- [23] Massimiliano Mancini, Muhammad Ferjad Naeem, Yongqin Xian, and Zeynep Akata. Learning graph embeddings for open world compositional zero-shot learning. *IEEE Transactions on Pattern Analysis and Machine Intelligence*, 46(3): 1545–1560, 2024. doi: 10.1109/TPAMI.2022.3163667. 2
- [24] Chao Jia, Yinfei Yang, Ye Xia, Yi-Ting Chen, Zarana Parekh, Hieu Pham, Quoc Le, Yun-Hsuan Sung, Zhen Li, and Tom Duerig. Scaling up visual and vision-language representation learning with noisy text supervision. In Marina Meila and Tong Zhang, editors, *Proceedings of the 38th International Conference on Machine Learning*, volume 139 of *Proceedings of Machine Learning Research*, pages 4904–4916. PMLR, 18–24 Jul 2021. URL <https://proceedings.mlr.press/v139/jia21b.html>. 2
- [25] Maria Parelli, Alexandros Delitzas, Nikolas Hars, Georgios Vlassis, Sotirios Anagnostidis, Gregor Bachmann, and Thomas Hofmann. Clip-guided vision-language pre-training for question answering in 3d scenes. In *2023 IEEE/CVF Conference on Computer Vision and Pattern Recognition Workshops (CVPRW)*, pages 5607–5612, 2023. doi: 10.1109/CVPRW59228.2023.00593. 2
- [26] Zequn Zeng, Hao Zhang, Zhengjue Wang, Ruiying Lu, Dongsheng Wang, and Bo Chen. Conzic: Controllable zero-shot image captioning by sampling-based polishing. *arXiv preprint arXiv:2303.02437*, 2023. 2
- [27] Alec Radford, Jong Wook Kim, Chris Hallacy, Aditya Ramesh, Gabriel Goh, Sandhini Agarwal, Girish Sastry, Amanda Askell, Pamela Mishkin, Jack Clark, Gretchen Krueger, and Ilya Sutskever. Learning transferable visual models from natural language supervision. In Marina Meila and Tong Zhang, editors, *Proceedings of the 38th International Conference on Machine Learning*, volume 139 of *Proceedings of Machine Learning Research*, pages 8748–8763. PMLR, 18–24 Jul 2021. URL <https://proceedings.mlr.press/v139/radford21a.html>. 2
- [28] Tom Brown, Benjamin Mann, Nick Ryder, Melanie Subbiah, Jared D Kaplan, Prafulla Dhariwal, Arvind Neelakantan, Pranav Shyam, Girish Sastry, Amanda Askell, Sandhini Agarwal, Ariel Herbert-Voss, Gretchen Krueger, Tom Henighan, Rewon Child, Aditya Ramesh, Daniel Ziegler, Jeffrey Wu, Clemens Winter, Chris Hesse, Mark Chen, Eric Sigler, Mateusz Litwin, Scott Gray, Benjamin Chess, Jack Clark, Christopher Berner, Sam McCandlish, Alec Radford, Ilya Sutskever, and Dario Amodei. Language models are few-shot learners. In H. Larochelle, M. Ranzato, R. Hadsell, M.F. Balcan, and H. Lin, editors, *Advances in Neural Information Processing Systems*, volume 33, pages 1877–1901. Curran Associates, Inc., 2020. URL https://proceedings.neurips.cc/paper_files/paper/2020/file/1457c0d6bfc4967418bfb8ac142f64a-Paper.pdf. 2
- [29] Zhengyuan Yang, Zhe Gan, Jianfeng Wang, Xiaowei Hu, Yumao Lu, Zicheng Liu, and Lijuan Wang. An empirical study of gpt-3 for few-shot knowledge-based vqa. In *AAAI*, 2022. 2
- [30] Thomas N Kipf and Max Welling. Semi-supervised classification with graph convolutional networks. *arXiv preprint arXiv:1609.02907*, 2016. 4
- [31] Kaiyang Zhou, Jingkang Yang, Chen Change Loy, and Ziwei Liu. Learning to prompt for vision-language models. *International Journal of Computer Vision (IJCV)*, 2022. 5, 6, 4
- [32] Phillip Isola, Joseph J. Lim, and Edward H. Adelson. Discovering states and transformations in image collections. In *2015 IEEE Conference on Computer Vision and Pattern Recognition (CVPR)*, pages 1383–1391, 2015. doi: 10.1109/CVPR.2015.7298744. 5
- [33] Aron Yu and Kristen Grauman. Fine-grained visual comparisons with local learning. In *2014 IEEE Conference on Computer Vision and Pattern Recognition*, pages 192–199, 2014. doi: 10.1109/CVPR.2014.32. 5
- [34] Tian Zhang, Kongming Liang, Ruoyi Du, Xian Sun, Zhanyu Ma, and Jun Guo. Learning invariant visual representations for compositional zero-shot learning. In Shai Avidan, Gabriel Brostow, Moustapha Cissé, Giovanni Maria Farinella, and Tal Hassner, editors, *Computer Vision – ECCV 2022*, pages 339–355, Cham, 2022. Springer Nature Switzerland. ISBN 978-3-031-20053-3. 7
- [35] Ishan Misra, Abhinav Gupta, and Martial Hebert. From red wine to red tomato: Composition with context. In *2017 IEEE Conference on Computer Vision and Pattern Recognition (CVPR)*, pages 1160–1169, 2017. doi: 10.1109/CVPR.2017.129. 4
- [36] Senthil Purushwalkam, Maximillian Nickel, Abhinav Gupta, and Marc’auelio Ranzato. Task-driven modular networks for zero-shot compositional learning. In *2019 IEEE/CVF International Conference on Computer Vision (ICCV)*, pages 3592–3601, 2019. doi: 10.1109/ICCV.2019.00369. 4
- [37] Yong-Lu Li, Yue Xu, Xiaohan Mao, and Cewu Lu. Symmetry and group in attribute-object compositions. In *IEEE/CVF Conference on Computer Vision and Pattern Recognition (CVPR)*, June 2020. 4
- [38] Muhammad Umer Anwaar, Zhihui Pan, and Martin Kleinteuber. On leveraging variational graph embeddings for open world compositional zero-shot learning. In *Proceedings of the 30th ACM International Conference on Multimedia*, MM ’22, page 4645–4654, New York, NY, USA, 2022. Association for Computing Machinery. ISBN 9781450392037. doi: 10.1145/3503161.3547798. URL <https://doi.org/10.1145/3503161.3547798>. 4
- [39] Qingsheng Wang, Lingqiao Liu, Chenchen Jing, Hao Chen, Guoqiang Liang, Peng Wang, and Chunhua Shen. Learning

- conditional attributes for compositional zero-shot learning. In *2023 IEEE/CVF Conference on Computer Vision and Pattern Recognition (CVPR)*, pages 11197–11206, 2023. doi: 10.1109/CVPR52729.2023.01077. 4
- [40] Muhammad Gul Zain Ali Khan, Muhammad Ferjad Naeem, Luc Van Gool, Alain Pagani, Didier Stricker, and Muhammad Zeshan Afzal. Learning attention propagation for compositional zero-shot learning. In *Proceedings of the IEEE/CVF Winter Conference on Applications of Computer Vision (WACV)*, pages 3828–3837, January 2023. 4
- [41] Henan Wang, Muli Yang, Kun Wei, and Cheng Deng. Hierarchical prompt learning for compositional zero-shot recognition. In *Proceedings of the Thirty-Second International Joint Conference on Artificial Intelligence, IJCAI '23*, 2023. ISBN 978-1-956792-03-4. doi: 10.24963/ijcai.2023/163. URL <https://doi.org/10.24963/ijcai.2023/163>. 4
- [42] Yun Li, Zhe Liu, Saurav Jha, and Lina Yao. Distilled reverse attention network for open-world compositional zero-shot learning. In *Proceedings of the IEEE/CVF International Conference on Computer Vision (ICCV)*, pages 1782–1791, October 2023. 4

Duplex: Dual Prototype Learning for Compositional Zero-Shot Learning

Supplementary Material

6. Comparison with Existing CZSL Methods

Dataset. We experiment with three real-world CZSL benchmarks: MIT-States, UT-Zappos, and CGQA. We summarize detailed statistics in Tab. 7

		UT-Zappos	MIT-States	CGQA
<i>Attribute</i>		16	115	413
<i>Object</i>		12	245	674
<i>Attr. × Obj.</i>		192	28175	278362
Train	Pair	83	1262	5592
	Image	22998	30338	26920
Validation	Seen Pair	15	300	1252
	Unseen Pair	15	300	1040
	Image	3214	10420	7280
Test	Seen Pair	18	400	888
	Unseen Pair	18	400	923
	Image	2914	19191	5098

Table 7. Dataset Statistics for MIT-States, UT-Zappos and CGQA.

Baselines. We compare our model with CLIP-based and existing CZSL methods with a pre-trained ResNet-18 backbone. For CompCos and Co-CGE, we report the results of which version of the models according to the experimental setup, i.e., the closed-world version for the closed-world setting, and the open-world version for the open-world setting.

Results. In the main text, we primarily present the performance comparison results between *Duplex* and a series of advanced CLIP-based approaches. Here, we report more extensive comparison results by including a variety of representative traditional methods as well. The evaluation results for closed-world and open-world settings are listed in Table 9 and Table 10, respectively.

It can be observed that, benefiting from the encyclopedic knowledge acquired through pre-training, the CLIP-based methods significantly outperform those that do not use pre-trained models in both settings.

7. Implementation Details

In this section, we give more details about the architecture, training and evaluation for reference.

7.1. Hyperparameters

Table 8 lists the hyperparameters that differ on each dataset And the determination is based on the validation performance.

For other hyperparameters, the pre-trained word embeddings "a photo of" in CLIP are used to initialize all three prefixes. For the adapter inserted into the image encoder, the bottleneck dimension r is set to 64, and the dropout rate is set to 0.1. During training, we use the *Adam* optimizer and reduce the learning rate of all trainable parameters by 0.5 every 5 epochs.

Hyperparameter	MIT-States	UT-Zappos	CGQA
Learning rate	10^{-4}	5×10^{-4}	1.5×10^{-5}
Batch size	128	128	64
Number of epochs	15	20	20
graph node dimension	768	768	768
state&object disentangler dimension	768	768	768

Table 8. Hyperparameters for different datasets.

7.2. Hyperparameter Sensitivity Analysis

In this section, we vary some key hyperparameters to examine how sensitive the proposed Duplex is to them.

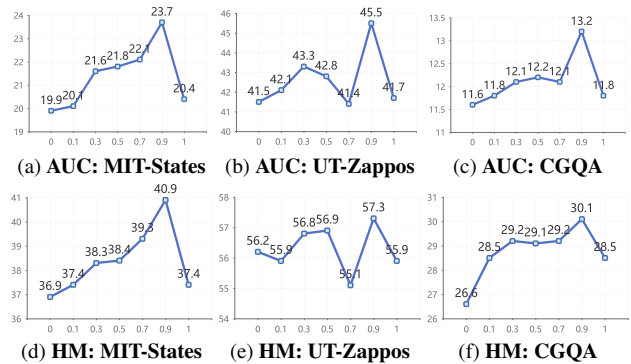


Figure 6. Sensitivity analysis on Graph update value of λ

Initialization of λ In Fig. 6, we examine the effect of varying the update state and object node features for composition by altering the initial value of the parameter vector λ , which regulates the update speed. Across all three datasets, initializing λ at 0.9 achieves the highest AUC, with performance improving progressively until this optimal value. Beyond this point, performance declines as the vector increasingly relies on CLIP-initialized features for visual prototypes. This decline is attributed to slower updates of state and object node features, which reinforce the pre-training alignment established by visual prototypes. However, fully pre-trained CLIP-initialized features that remain fixed during training hinder the optimization of visual prototypes, thereby affecting performance.

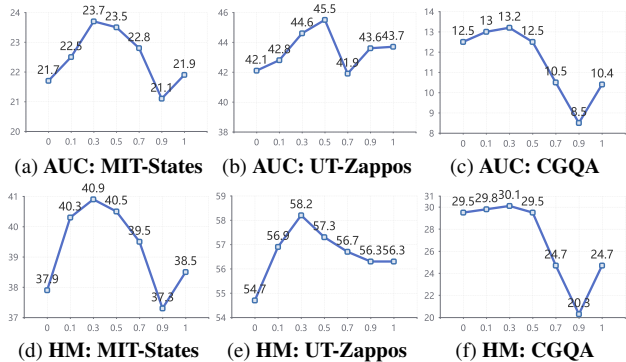


Figure 7. Sensitivity analysis on Initialization of the trainable semantic-visual prototype parameter vector α

Initialization of the trainable parameter γ vector The results for both datasets are presented in Tab. 3., where the visual prototype(VP) coefficients (γ) and semantic prototype(SP) coefficients ($1 - \gamma$) are learned during the training process. This section analyzes the impact of initializing the learnable weight coefficient γ on the configurations of visual and semantic prototypes. As shown in Figure 7, γ is varied from 0 to 1 in the combinatorial branch. When $\gamma=0$, only semantic prototypes are utilized, whereas $\gamma=1$ signifies the use of only visual prototypes. For the UT-Zappos dataset, the optimal performance is achieved in the closed-world setting when $\gamma=0.5$. Conversely, for MIT-States and CGQA, the best performance is observed at $\gamma=0.3$. We hypothesize that for non-domain-specific datasets, visual prototypes exhibit higher uncertainty, and excessive reliance on them may hinder the model’s ability to comprehend combinations effectively. In both scenarios, significant performance degradation occurs when $\gamma=0$ or $\gamma=1$, underscoring the need for appropriately initializing γ to balance visual and semantic prototypes in the Duplex method.

8. More visualizations

To conduct a more comprehensive qualitative analysis, as shown in Fig. 8, we present the visualization results of visual and semantic prototypes across three datasets, along with the embeddings of the test samples. Different colors represent distinct combination categories. From the embedding visualizations, it is evident that visual prototypes (\triangle) are closer to the cluster centers of the test sample (\circ) categories, while semantic prototypes (\square) are generally farther from the cluster centers. However, they provide complementary features to the visual prototypes, as demonstrated in the 145th category of the MIT-State dataset, where the semantic prototype is closer to the cluster center. These visualizations suggest that the Duplex method we propose can more effectively extract state and object features and robustly learn their corresponding compositions.

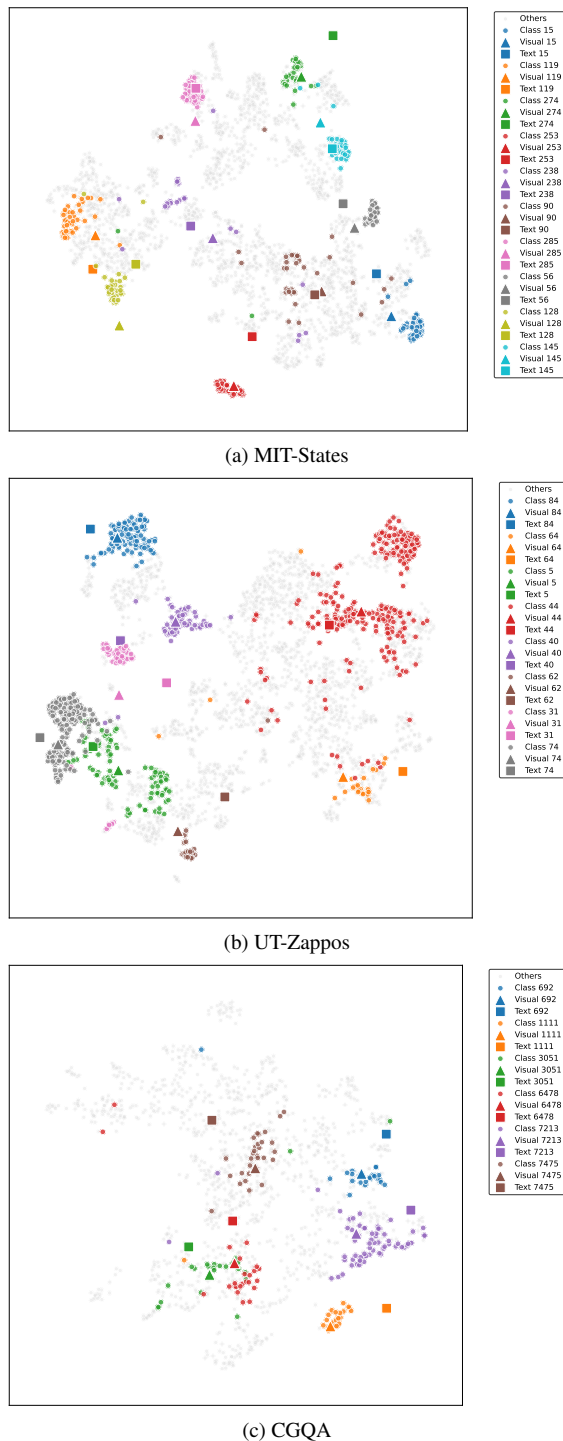
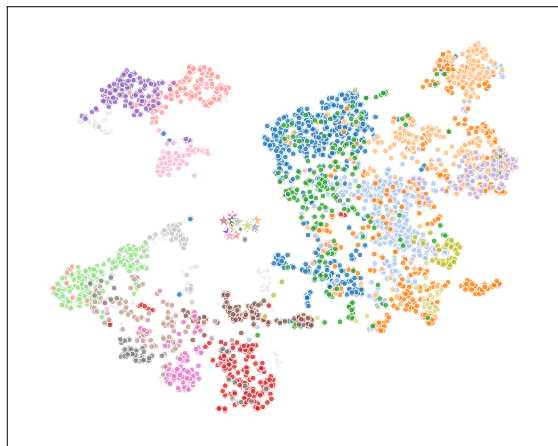


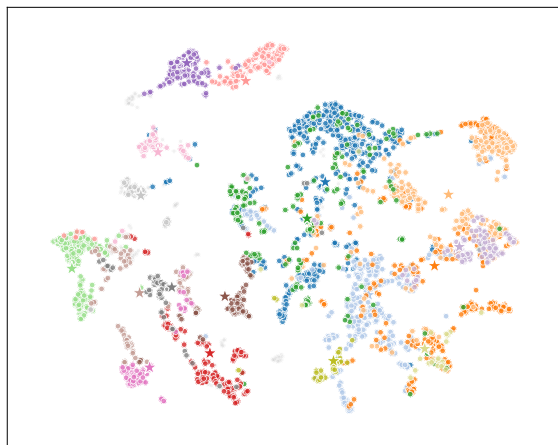
Figure 8. Visualization of visual/semantic prototypes and test samples embeddings in three datasets

Figure 9 presents the 2D embedding results of the UT-Zappos test samples using the Duplex method. Each point represents an individual image, with \star denoting the visual prototype. Each color corresponds to a category, and the 20

categories with the largest sample sizes were selected for visualization. In composition classification, representations with a high degree of separation are more discriminative. The proximity of \star to the clustering center reflects the visual prototype's ability to effectively separate composition categories. Visually, the trained Duplex exhibits improved grouping of visual prototypes across different image categories compared to the pre-training state. This improvement is attributed to Duplex's capacity to produce more distinguishable composition features by aggregating visual prototypes into composition information about similar category pairs. These results indicate that leveraging visual prototypes enhances the model's ability to differentiate between categories. However, Duplex still faces challenges in distinguishing strongly coupled categories, underscoring a crucial area for future refinement.



(a) Before Training



(b) After Training

Figure 9. Visualized clustering effects of test set samples from the UT-Zappos dataset before and after training.

Method	MIT-States				UT-Zappos				CGQA			
	S	U	HM	AUC	S	U	HM	AUC	S	U	HM	AUC
AoP[3]	14.3	17.4	9.9	1.6	59.8	54.2	40.8	25.9	17.0	5.6	5.9	0.7
LE+[35]	15.0	20.1	10.7	2.0	53.0	61.9	41.0	25.7	18.1	5.6	6.1	0.8
TMN[36]	20.2	20.1	13.0	2.9	58.7	60.0	45.0	29.3	23.1	6.5	7.5	1.1
SymNet [37]	24.2	25.2	16.1	3.0	49.8	57.4	40.4	23.4	26.8	10.3	11.0	2.1
CompCos [6]	25.3	24.6	16.4	4.5	59.8	62.5	43.1	28.1	28.1	11.2	12.4	2.6
CGE [7]	28.7	25.3	17.2	5.1	56.8	63.6	41.2	26.4	28.1	10.1	11.4	2.3
Co-CGE [8]	27.8	25.2	17.5	5.1	58.2	63.3	44.1	29.1	29.3	11.9	12.7	2.8
SCEN [11]	29.9	25.2	18.4	5.3	63.5	63.1	47.8	32.0	28.9	12.1	12.4	2.9
CVGAE [38]	28.5	25.5	18.2	5.3	65.0	62.4	49.8	34.6	28.2	11.9	13.9	2.8
CANet [39]	29.0	26.2	17.9	5.4	61.0	66.3	47.3	33.1	30.0	13.2	14.5	3.3
CAPE [40]	30.5	26.2	19.1	5.8	60.4	67.4	45.5	31.3	32.9	15.6	16.3	4.2
ADE [13]	—	—	—	—	63.0	64.3	51.1	35.1	35.0	17.7	18.0	5.2
CLIP [14]	30.2	46.0	26.1	11.0	15.8	49.1	15.6	5.0	7.5	25.0	8.6	1.4
CoOp [31]	34.4	47.6	29.8	13.5	52.1	49.3	34.6	18.8	20.5	26.8	17.1	4.4
CSP [15]	46.6	49.9	36.3	19.4	64.2	66.2	46.6	33.0	28.8	26.8	20.5	6.2
HPL [41]	47.5	50.6	37.3	20.2	63.0	68.8	48.2	35.0	30.8	28.4	22.4	7.2
GIPCOL [16]	48.5	49.6	36.6	19.9	65.0	68.5	48.8	36.2	31.92	28.4	22.5	7.14
DFSP(i2t) [17]	47.4	52.4	37.2	20.7	64.2	66.4	45.1	32.1	35.6	29.3	24.3	8.7
DFSP(BiF) [17]	47.1	52.8	37.7	20.8	63.3	69.2	47.1	33.5	36.5	32.0	26.2	9.9
DFSP(t2i) [17]	46.9	52.0	37.3	20.6	66.7	71.7	47.2	36.0	38.2	32.0	27.1	10.5
Troika [18]	49.0	53.0	39.3	22.1	66.8	73.8	54.6	41.7	41.0	35.7	29.4	12.4
Duplex(ours)	49.7	55.6	40.9	23.7	70.2	74.7	57.3	45.5	41.1	36.2	30.1	13.2

Table 9. Numerical results of different methods on three benchmark datasets under the **closed-world** setting.

Method	MIT-States				UT-Zappos				CGQA			
	S	U	HM	AUC	S	U	HM	AUC	S	U	HM	AUC
AoP[3]	16.6	5.7	4.7	0.7	50.9	34.2	29.4	13.7	-	-	-	-
LE+[35]	14.2	2.5	2.7	0.3	60.4	36.5	30.5	16.3	19.2	0.7	1.0	0.08
TMN[36]	12.6	0.9	1.2	0.1	55.9	18.1	21.7	8.4	-	-	-	-
SymNet [37]	21.4	7.0	5.8	0.8	53.3	44.6	34.5	18.5	26.7	2.2	3.3	0.43
CompCos [6]	25.4	10.0	8.9	1.6	59.3	46.8	36.9	21.3	28.4	1.8	2.8	0.39
CGE [7]	29.6	4.0	4.9	0.7	58.8	46.5	38.0	21.5	28.3	1.3	2.2	0.30
Co-CGE [8]	26.4	10.4	10.1	2.0	60.1	44.3	38.1	21.3	28.7	1.6	2.6	0.37
KG-SP	28.4	7.5	7.4	1.3	61.8	52.1	42.3	26.5	31.5	2.9	4.7	0.78
CVGAE [38]	27.3	9.9	10.0	1.8	58.6	48.4	41.7	22.2	26.6	2.9	6.4	0.7
ADE [13]	—	—	—	—	62.4	50.7	44.8	27.1	35.1	4.8	7.6	1.4
DRANet [42]	29.8	7.8	7.9	1.5	65.1	54.3	44.0	28.8	31.3	3.9	6.0	1.1
CLIP [14]	30.1	14.3	12.8	3.0	15.7	20.6	11.2	2.2	7.5	4.6	4.0	0.27
CoOp [31]	34.6	9.3	12.3	2.8	52.1	31.5	28.9	13.2	21.0	4.6	5.5	0.70
CSP [15]	46.3	15.7	17.4	5.7	64.1	44.1	38.9	22.7	28.7	5.2	6.9	1.20
HPL [41]	46.4	18.9	19.8	6.9	63.4	48.1	40.2	24.6	30.1	5.8	7.5	1.4
GIPCOL [16]	48.5	16.0	17.9	6.3	65.0	45.0	40.1	23.5	31.6	5.5	7.3	1.30
DFSP(i2t)[17]	47.2	18.2	19.1	6.7	64.3	53.8	41.2	26.4	35.6	6.5	9.0	1.95
DFSP(BiF) [17]	47.1	18.1	19.2	6.7	63.5	57.2	42.7	27.6	36.4	7.6	10.6	2.39
DFSP(t2i)[17]	47.5	18.5	19.3	6.8	66.8	60.0	44.0	30.3	38.3	7.2	10.4	2.40
Troika [18]	48.8	18.7	20.1	7.2	66.4	61.2	47.8	33.0	40.8	7.9	10.9	2.70
Duplex(ours)	49.5	20.3	21.8	8.3	70.2	62.4	49.6	35.4	41.6	9.2	12.5	3.9

Table 10. Numerical results of different methods on three benchmark datasets under the **open-world** setting.